P2.26 A CHARACTERIZATION OF COLD POOLS BELOW MARINE TRADE WIND CUMULI

Jørgen B. Jensen

Earth Observation Laboratory, National Center for Atmospheric Research, Boulder, Colorado

1. INTRODUCTION

Trade wind cumulus clouds form in an environment of limited external forcing. Typically they evolve in response to slowly varying external factors, such as fluxes from sea-surface, radiative cooling, convergence and divergence. Some times the trade wind clouds form cloud streets in response to wind shear, and at other times they form more irregular clumps on the mesoscale.

Trade-wind cumuli cover the spectrum from essentially non-precipitating to intensely precipitating clouds. Evaporation of precipitation forms cold pools below the clouds, and these cold pools may spread out and organize the formation of new convection. This process was observed in a shallow marine stratocumulus-cumulus occurrence over the Southern Ocean near Australia (Jensen et al., 2000). This situation had cumulus cloud bases of 550-600 m; i.e. similar to those observed during the 2004-2005 Rain in Cumulus over the Oceans (RICO) experiment off Antigua.

The Australian case had evaporatively formed cold pools with virtual temperatures more than 1 °C colder than the remainder of the mixed layer. The evolution of the cold pools were modeled by Jensen et al. (2000) using a simple internal boundary layer to estimate the time required for heating the cold pool to the same temperature as the remainder of the mixed layer.

Very little statistics is available on the frequency, size and other properties of precipitation generated cold pools. The purpose of this study is to examine the characteristics of cold pools over the Caribbean as observed during the RICO experiment.

2. OBSERVATIONS

Almost all the RICO flight time was devoted to statistical properties of the cumulus clouds. RICO flights were conducted with the NCAR/NSF C-130 research aircraft on 19 days during December 2004 and January 2005. On most days, the flights would include circular flight tracks at about 85 m above sea surface at the beginning and end of the flights. A total of 33 such circles, each lasting about 30 minutes forms the basis for the following analysis. The flight tracks formed circles with a diameter of about 60 km, and these circles were conducted in a regular manner without regard to precipitation, cold pools, and the presence or absence of clouds. Thus the 33 circles represent an unbiased sample of cold pools and the remainder of the mixed layer. For simplicity, we will here call the remainder of the mixed layer for the 'warm regions'.

There is no objective way to determine a criterion for what constitutes a cold pool and a warm region; a few examples will demonstrate that for individual cases we can examine the distribution of virtual potential temperature and clearly see what constitutes cold pools, but to generalize this is difficult. Figures 1 and 2 show time series of virtual potential temperature, θ_v and precipitation water content, $PLWC$. In Fig. 1 (research flight RF04, circle 2), the curve shows no apparent cold pools, whereas Fig. 2 (RF15, circle 2) shows two apparent cold pools. In calculating θ_v we use the C-130 variable PSXC for pressure, and for temperature we use the Ophir radiometer temperature variable, OAT. For circles with intermittent Ophir radiometer data, we use the normal Rosemount variable, ATX, for temperature. The reason for use of the Ophir temperature instead of the Rosemount temperature variable is that the Rosemount temperature sensor can show wetting-induced cooling in precipitation regions; this temperature wetting artifact has previously been demonstrated by Lenschow and Pennell (1974) for cloudy regions. In the calculation of θ_v we use the dewpoint values from one of the Lyman-α sensors.

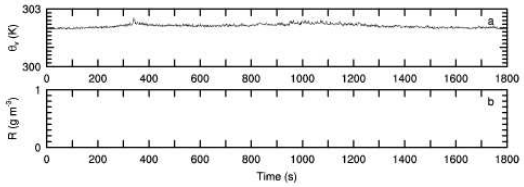

Figure 1. Time series of virtual potential temperature, (θ_v, above), and precipitation water content ($PLWC$, below) for RF04, circle 2. During the flight of this circle, no precipitation was observed.

Corresponding author address: Jørgen B. Jensen, NCAR/EOL/RAF, P. O. Box 3000, Boulder, CO 80307

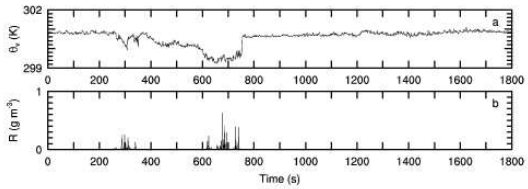

Figure 2. Same as Figure 1, but for RF15, circle 2. During the flight of this circle, considerable precipitation was observed and this occurred in the regions with lowered θ_v.

The 1800 1-second samples for a circle were ranked in order of decreasing θ_v. Figures 3 and 4 show cumulative percentiles of 1-second samples with temperatures higher than the listed value of θ_v. The median θ_v is thus given by the 50% percentile. Figure 3 shows a nearly symmetric distribution of the θ_v values, whereas Fig. 4 shows a 'break' in the distribution at a percentile value of about 75%. The break occurs in this case at a temperature of a few tenths below the median θ_v, and samples to the right side of the break show cooling of up to 1.4 °C compared to the remainder of the samples.

3. COLD POOL θ_v DISTRIBUTIONS

In order to generalize the cold-pool determination for the 33 circles, we will somewhat arbitrarily define cold-pool air as having a value of θ_v that is cooled by

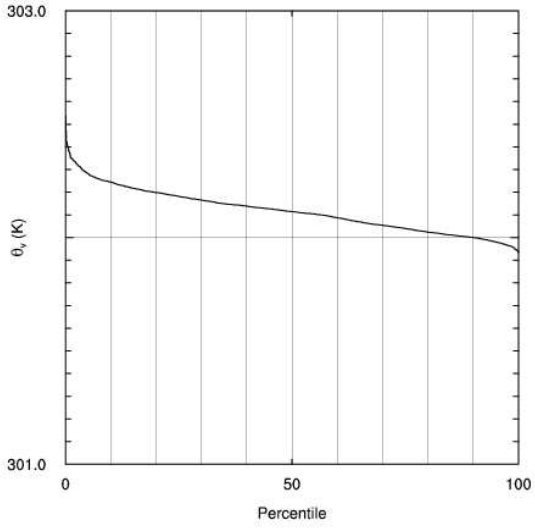

Figure 3. Ranked distribution of virtual potential temperature, θ_v, for RF07, circle 1. The nearly symmetric distribution shows no obvious evidence of evaporation formed cold pools.

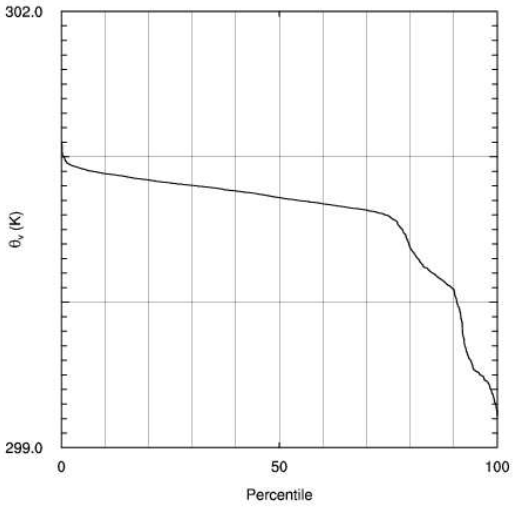

Figure 4. Ranked distribution of virtual potential temperature, θ_v, for RF15, circle 2. The distribution shows a clear break in the distribution around 75%, which suggests evaporation-formed cold pools.

at least 0.5 °C from the median θ_v. The result is that 16 of the circles qualify as having cold pools, and that 17 do not contain any cold pools; i.e. roughly half of the circles of 200 km flight length contain cold pools.

The ranked θ_v data can be normalized to display only the deviations in θ_v from the median value. We do this for the 17 circles without cold pools (Fig. 5) and for the 16 circles with cold pools (Fig. 6). The circles without cold-pool characteristics show a very narrow distribution around the median θ_v value. In contrast, the circles with cold pool signatures show a much wider range of θ_v values, in particular in the cold pools; however, this widening of the distribution is also evident as higher θ_v values in the warmest parts of circles containing cold pools. Thus the mixed-layers with disturbed conditions (cold pools) also frequently show elevated temperatures in the warmest regions.

4. SIZES OF COLD POOLS

Further analysis was done to determine the sizes of contiguous regions with cooling of at least 0.5 degrees relative to the circle median θ_v. Taking RF15 circle 2 as an example, we show in Figs. 7 and 8 the ranked sizes of cold pools and warm regions, respectively, with the largest contiguous region on the left side of the diagram. Figure 7 shows one cold pool with dimension of about 18 km, the second largest being only about 3 km, etc. The right half of the figure contains regions defined as cold pools even if these only contain

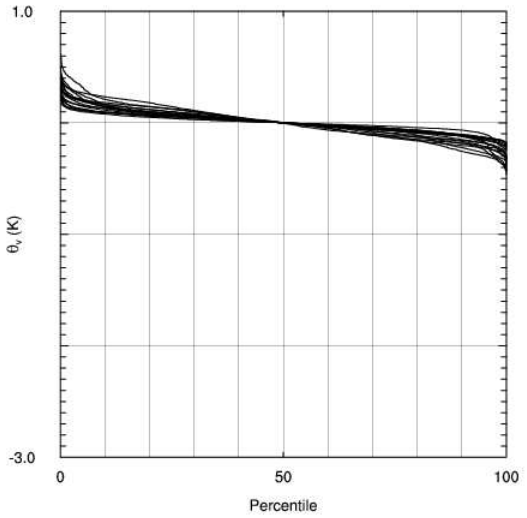

Figure 5. Ranked and normalized distribution of virtual potential temperature, θ_v, for the 17 RICO near-surface circles without evidence of cold pools.

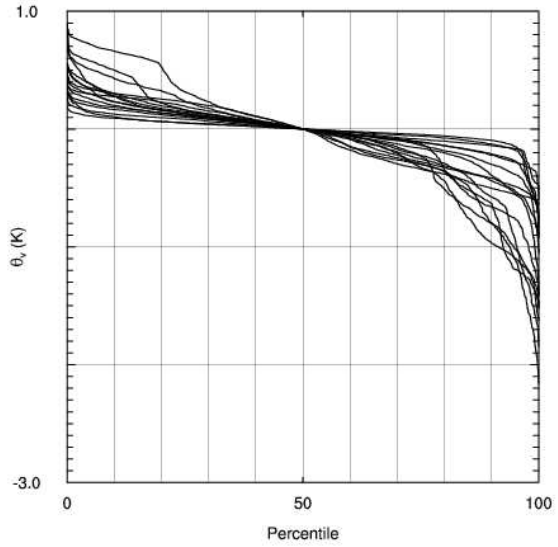

Figure 6. Ranked and normalized distribution of virtual potential temperature, θ_v, for the 16 RICO near-surface circles with evidence of cold pools.

one or a few seconds of measurements. In this figure, as well as in the following ones, the focus should be on the left part of the figure which demonstrates large contiguous cold pools.

Figure 8 shows the same information for the warm regions. Here the picture is once again dominated by large contiguous warm regions, see the left part of the figure.

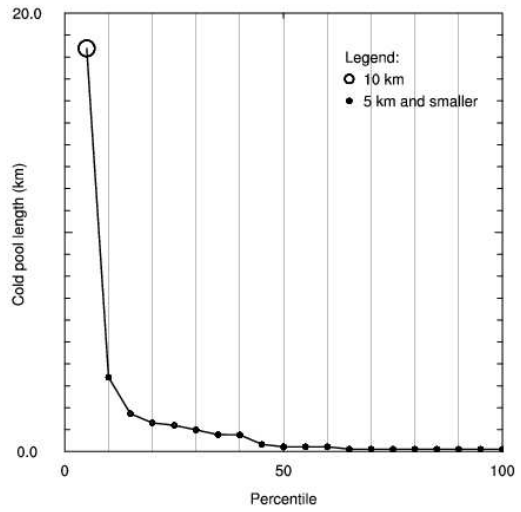

Figure 7. Ranked sizes of the cold pools observed during RF15, circle 2.

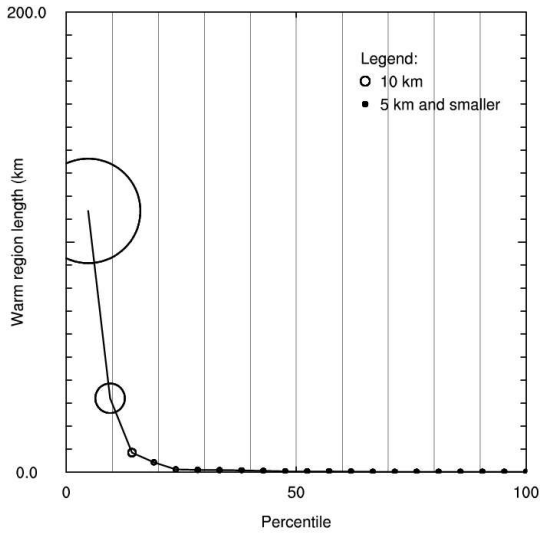

Figure 8. Ranked sizes of the warm regions observed during RF15, circle 2.

Figures 9 and 10 shows the average θ_v for the size-ranked cold pools and and warm regions, respectively. The largest warm regions and cold sectors fall in separate ends of the spectrum.

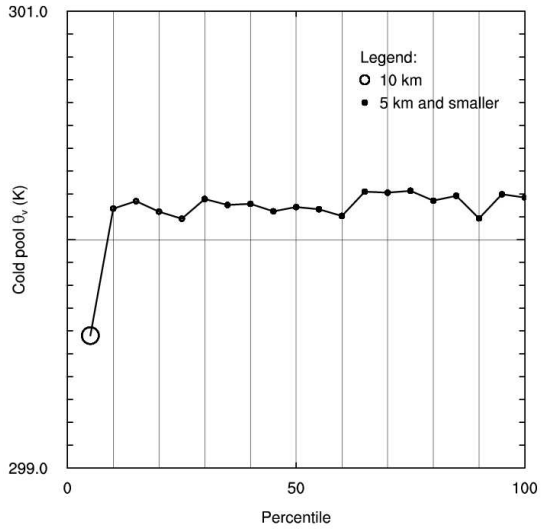

Figure 9. Average θ_v for size-ranked cold pools observed during RF15, circle 2.

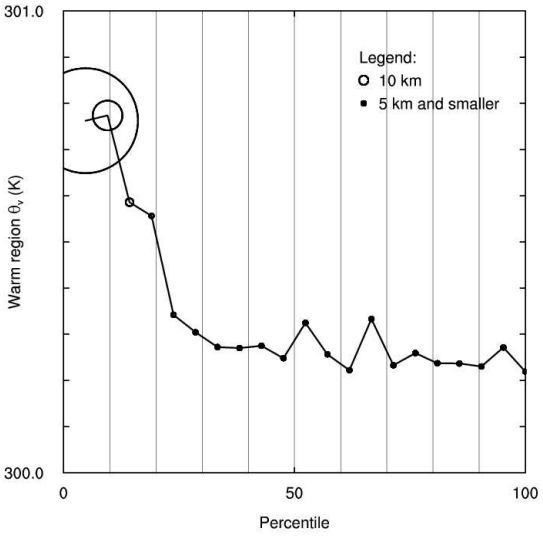

Figure 10. Average θ_v for size-ranked warm regions observed during RF15, circle 2.

If a cold pool is formed by precipitation falling into the mixed layer, then cooling leads to more dense air in the mixed layer and more dense air should lead to a locally higher air pressure, all other things being equal. Pressure perturbations can be examined by first considering the D-value (LeMone and Tarleton, 1986), that is the difference between the actual altitude of the aircraft (z_{gps}) and the pressure altitude of the aircraft (z_p) which in the data set is defined based on the US Standard Atmosphere. Thus:

$$D = z_{gps} - z_p \qquad (1)$$

The actual value of D is not significant for our analysis; rather it is the variation of D along the flight track that is the basis for calculating pressure perturbations, p'. From the hydrostatic equation, we have:

$$p' = (D - \bar{D})\rho_a g \qquad (2)$$

where ρ_a is the air density and g is the gravity acceleration. The cold pool and warm region averages of pressure perturbations are shown in Figs. 11 and 12. The largest warm region has nearly no average pressure perturbation; this is to be expected as it contributes heavily to defining the background pressure. In contrast, the largest cold pool (which is about a factor 10 smaller) has a considerable positive pressure perturbation of about 30 Pa (or 0.3 hPa). A higher pressure should lead to divergence within the cold pool air, and this may lead to convergence outside the cold pool, thus potentially providing the forcing for new convection. An average high-pressure perturbation of 0.3 mb over 18km we consider highly significant. This value is larger than observed at cloud base of continental clouds by LeMone et al. (1988a, clouds in low wind shear), but smaller than that observed at cloud base in deep continental clouds (LeMone et al., 1988b).

A companion paper, Jensen et al. (2006, this volume), examines pressure perturbations below and in clouds, as well as the simultaneous convergence/divergence fields and wind speeds.

4. CONCLUSIONS

In this preliminary study of could pools observed about 85 m over the Caribbean Ocean off the coast of Antigua we have examined 33 circles with diameters of about 60 km. The track length along the circle is thus

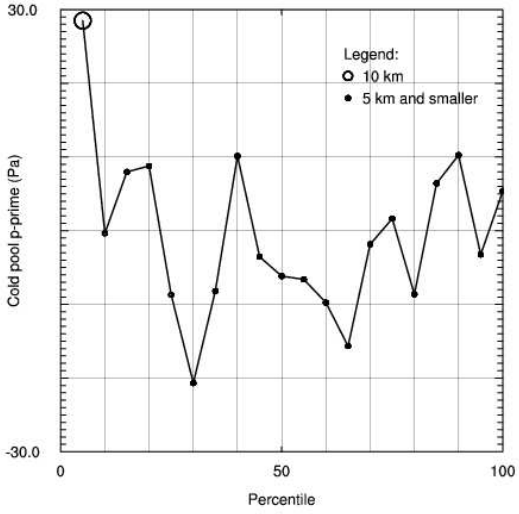

Figure 11. Average pressure perturbations, $\bar{p'}$, for size-ranked cold pools observed during RF15, circle 2.

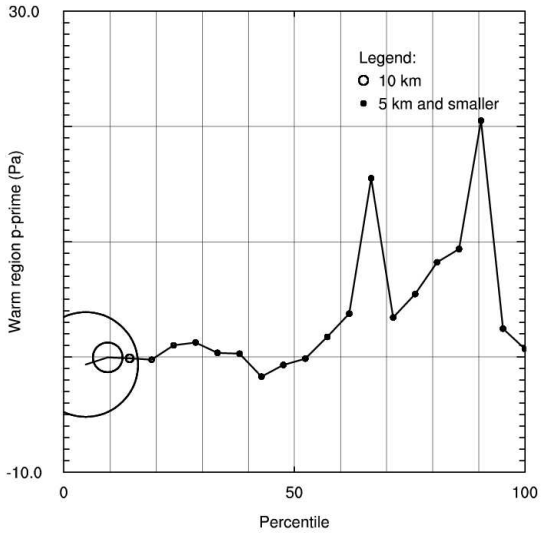

Figure 12. Average pressure perturbations, $\bar{p}'$, for size-ranked warm regions observed during RF15, circle 2.

about 200 km. We defined, somewhat arbitrarily, cold pools as being regions with a virtual potential temperature of at least 0.5 °C cooler than the circle median temperature.

- About half the circles contain samples with a temperature qualifying for a cold pool. The cold pools cover a relatively small fraction of the total flight tracks, typically less than 10% of the total track length.
- By ranking the 1800 1-second samples in order of descending θ_v values, it was found that the 17 circles without cold pools showed an almost symmetric distribution of θ_v around the median θ_v value. In contract, the circles with cold pools showed a much more asymmetric distribution of θ_v. This was particularly the case for the cold pools, but it was also evident in the warm regions.
- Pressure perturbations in the larger cold pools may constitute a significant fraction of a millibar; this should be sufficient to initiate divergence in the cold pools.

It is hoped that the present statistical results can be used in evaluating predictions from large-eddy simulations and other model calculations. The cold pools are a dramatic feature of the sub-cloud marine boundary layer in the presence of precipitating cumuli. The observed statistics of cold pools should therefore also be evident in model results obtained with models that correctly predict the organization of and precipitation from trade wind cumuli.

No attempt has been made here on matching the observed cold pools and their divergence patterns to radar observations of cloud organization and development. A suitable radar, SPol, was operated on the island of Barbuda; such analysis we leave for further studies.

ACKNOWLEDGMENTS

Many thanks to Drs. Pavel Romashkin and Stuart Beaton for provision and calculation of the GPS data. NCAR is sponsored by the National Science Foundation.

REFERENCES

Jensen, J. B., S. Lee, P. B. Krummel, J. Katzfey and D. Gogoasa, 2000: Precipitation in marine cumulus and stratocumulus. Part I: Thermodynamic and dynamic observations of closed cell circulations and cumulus bands. *Atmos. Res.*, **54**, 117-155.

Jensen, J. B., P. Romashkin and S. Beaton, 2006: Pressure perturbations in and below trade wind cumulus clouds: Forcing patterns. *This volume.*

LeMone, A. M., and L. F. Tarleton, 1986: The use of inertial altitude in the determination of convective-scale pressure field over land. *J. Atmos. Ocean. Tech.*, **3**, 650-661.

LeMone, A. M., L. F. Tarleton, and G. M. Barnes, 1988a: Perturbation pressure at the base of cumulus clouds in low shear. *Mon. Wea. Rev.*, **116**, 2062-2068.

LeMone, A. M., G. M. Barnes, J. C. Fankhauser and L. F. Tarleton, 1988b: Perturbation pressure fields measured by aircraft around the cloud-base updraft of deep convective clouds. *Mon. Wea. Rev.*, **116**, 313-327.

Lenschow, D. H., and W. T. Pennell, 1974: On the measurements of in-cloud and wet-bulb temperature from an aircraft. *Mon. Wea. Rev.*, **102**, 447-454.